

TSFormer: A Robust Framework for Efficient UHD Image Restoration

Xin Su

Fuzhou University

suxin4726@gmail.com

Chen Wu

University of Science and Technology of China

wuchen5X@mail.ustc.edu.cn

Zhuoran Zheng*

Sun Yat-sen University

zhengzr@njust.edu.cn

Abstract

*Ultra-high-definition (UHD) image restoration is vital for applications demanding exceptional visual fidelity, yet existing methods often face a trade-off between restoration quality and efficiency, limiting their practical deployment. In this paper, we propose **TSFormer**, an all-in-one framework that integrates Trusted learning with Sparsification to boost both generalization capability and computational efficiency in UHD image restoration. The key is that only a small amount of token movement is allowed within the model. To efficiently filter tokens, we use Min- p with random matrix theory to quantify the uncertainty of tokens, thereby improving the robustness of the model. Our model can run a 4K image in real time (40fps) with 3.38 M parameters. Extensive experiments demonstrate that TSFormer achieves state-of-the-art restoration quality while enhancing generalization and reducing computational demands. In addition, our token filtering method can be applied to other image restoration models to effectively accelerate inference and maintain performance.*

1. Introduction

Ultra-high-definition (UHD) image restoration is essential for various applications that require high-resolution image quality, including medical imaging, video streaming, and digital surveillance [3, 17, 31, 36]. Since UHD images have millions of pixels, processing them with limited resources can be a huge challenge.

Currently, there are some deep learning frameworks [34, 39] that can process UHD images on consumer-grade GPUs. However, these methods directly or indirectly downsample the input image, and may lose some tokens that are important for image restoration. Therefore, this results in a

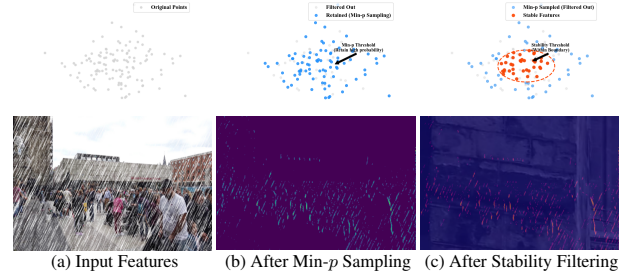


Figure 1. **Illustration of the Min- p sampling and stability filtering process.** (a) The original input image used as a reference. (b) Result after Min- p sampling, where high-probability regions are retained and highlighted in a distinct color, indicating sparsified yet significant areas. (c) Result after stability filtering, where only the stable, high-confidence features are preserved, with stable regions marked in red and unstable regions suppressed.

loss of detail in the image, which is particularly important for UHD images. To address this problem, we propose **TSFormer**, a lightweight and trusted framework that combines sparsification with random matrix theory. TSFormer is designed to retain only the most informative features, thereby significantly reducing computational overhead while maintaining high restoration quality and robustness.

Indeed, the first key component of TSFormer is **Min- p sampling**, a probability-driven sparsification technique inspired by recent advances in probabilistic sparsification theory [1]. Unlike conventional Top- k filtering methods [18], Min- p sampling selectively retains high-confidence features based on a probabilistic threshold, allowing dynamic feature selection. This “less is more” approach recognizes that not all features contribute equally to the final output, especially in high-dimensional data like UHD images. However, while Min- p sampling effectively reduces the model’s computational demands, it may introduce instability due to noise in the large number of tokens. To address this issue, TSFormer incorporates a **trusted** mechanism grounded in random matrix theory [7, 23]. This trusted

*Corresponding author.

filtering involves analyzing the eigenvalues of feature matrices to ensure that only robust, high-confidence features are retained. As shown in Figure 1(a), Min- p sampling applies a probability-based threshold to retain high-confidence features while discarding those of lower importance, achieving effective sparsification. In Figure 1(b), trusted filtering based on random matrix theory refines the remaining features further by excluding points outside a trusted threshold (dashed circle). This trusted-driven feature selection improves generalization, allowing the model to perform reliably across varied degraded images [10, 35]. So far, we have constructed a Min- p Sparse Attention (MSA) by enforcing a Min- p with a trusted mechanism, which efficiently and robustly generates an attention map. MSA is integrated into each block of the TSFormer, and each block also contains frequency domain learning and multi-scale learning components. TSFormer shows promising performance in multiple UHD image tasks and can run a UHD image in real time on resource-constrained devices (a single 3090 GPU shader with 24G RAM). In summary, our contributions are as follows:

- We develop a novel UHD image restoration model (TSFormer) that can run a 4K resolution image in real-time on a single GPU with strong generalization capabilities.
- We design a token filtering method with a trusted mechanism, which is integrated into the TSFormer to generate high-quality attention maps.
- The token filtering method with a trusted mechanism can be used in any Transformer-based image restoration framework to improve the efficiency of the model. Extensive experimental results show the effectiveness of our method.

2. Related Work

2.1. UHD Image Restoration

Ultra-high-definition (UHD) image restoration is essential for applications in medical imaging, video streaming, and digital surveillance [31, 36]. Recently, deep learning methods have efficiently reconstructed UHD images' details and colors through sampling and parallelization techniques. Zheng et al. [40] introduced a multi-guided bilateral upsampling model for UHD image dehazing, enhancing clarity through multiple guidance inputs. Deng et al. [6] developed a separable-patch integration network for UHD video deblurring, employing a multi-scale integration scheme to mitigate motion and blur artifacts. Wang et al. [26] proposed LLFormer, a transformer-based method for low-light enhancement utilizing axis-based multi-head self-attention and cross-layer attention fusion blocks to improve illumination and contrast. In addition, there are some methods [34, 39] to reconstruct clear UHD images in real time by building lightweight models and looking up tables.

Although these methods can enhance a UHD image in

real time, the sampling and table lookup methods are not supervised by a trusted mechanism, which limits the generalisation ability of the model. In contrast, our proposed TSFormer incorporates Min- p sampling for adaptive sparsification and employs trusted filtering based on random matrix theory [2, 9], enhancing both feature reliability and restoration quality while maintaining low computational costs.

2.2. Token Sampling Technology

Currently, large language models (LLM) use some token sampling techniques to speed up inference. Traditional methods like Top- k filtering [8, 18] prioritize features based on magnitude but use fixed thresholds that may not adapt to varying data distributions, potentially discarding valuable information. Probabilistic sparsification methods, such as Min- p sampling [1, 42], introduce dynamic, probability-based thresholds that better adapt to data distributions, allowing flexible feature retention. Inspired by this, we introduced the token technology to build an efficient model. On this basis, while ensuring real-time performance, a trusted mechanism (random matrix theory) is introduced to accurately sample tokens [4].

2.3. Random Matrix Theory

Trusted filtering of tokens is difficult, and it can lead to a significant slowdown in the speed of model inference. Compared to other approaches to trusted modeling such as Bayesian, variational inference, and labeled distributions, random matrix theory trades off the speed and accuracy of inference. Random matrix theory (RMT) offers a framework for analyzing and enhancing feature stability in high-dimensional data [7, 23]. By examining eigenvalue distributions, RMT-based methods can identify and retain the most stable and salient features, improving robustness and generalization [10, 35]. However, integrating RMT into deep learning for UHD restoration remains underexplored, presenting an opportunity to enhance feature reliability without significantly increasing computational costs.

3. Method

In this section, we introduce TSFormer, an efficient Transformer network for UHD image restoration. It is a symmetrical encoder and decoder structure, as shown in Figure 2.

3.1. Preliminaries

Min- p Sampling. Min- p sampling is a novel sampling method originally designed for large language model tasks, where it dynamically adjusts the sampling threshold to retain high-confidence tokens [20]. Specifically, given a set of logits \mathbf{L} within a patch, Min- p sampling applies a threshold defined as a proportion p_{base} of the maximum value in the feature patch:

$$\text{Threshold} = p_{\text{base}} \cdot \max(\mathbf{L}), \quad (1)$$

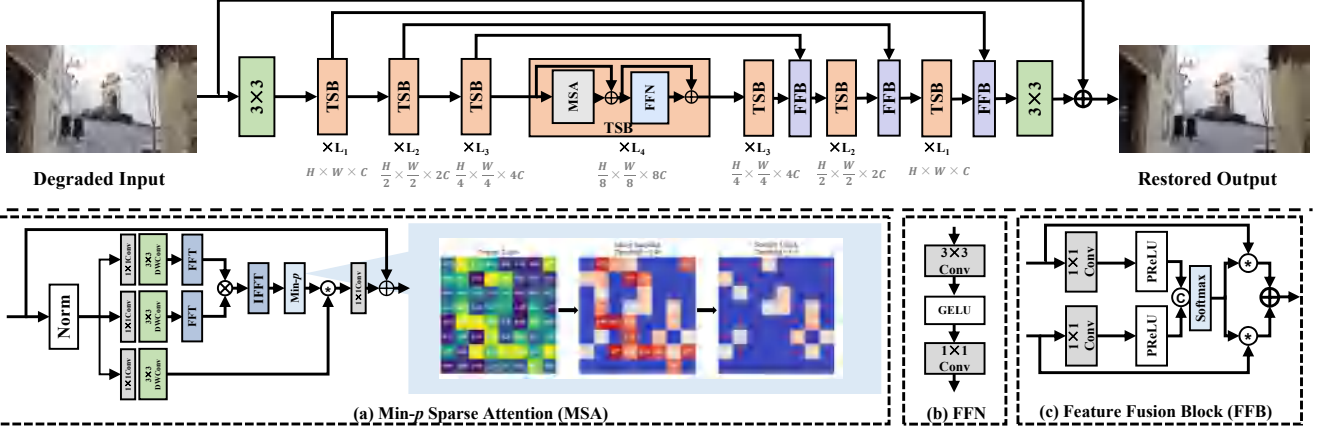


Figure 2. The overall architecture of the proposed TSFormer for UHD image restoration, which mainly consists of Trusted Sparse Blocks (TSB) and a Feed-forward Network (FFN). Our core is Min- p Sparse Attention (MSA), which incorporates the ability of dynamic token filtering and sparse representation, effectively reducing the burden of running a UHD image. In addition, MSA is also a plug-and-play algorithm that can be used in any image restoration network based on the Transformer architecture.

where $p_{\text{base}} \in [0, 1]$ is a hyperparameter that controls sparsity. This threshold filters out low-confidence features by setting elements in \mathbf{L} below the threshold to zero:

$$\mathbf{L}_{\text{sampled}} = \begin{cases} \mathbf{L}, & \text{if } \mathbf{L} \geq \text{Threshold}, \\ 0, & \text{otherwise.} \end{cases} \quad (2)$$

This method acts on the sparsification of the attention map to filter out unimportant features and noise.

Fast Fourier Transform. To further optimize the computational efficiency of our attention mechanism, we employ Fast Fourier Transform (FFT) for attention computation in the frequency domain. FFT significantly reduces the complexity of calculating attention scores, particularly for high-resolution images.

The forward Fourier transform of a 1D signal $x(t)$ is given by:

$$X(f) = \int_{-\infty}^{\infty} x(t) e^{-i2\pi ft} dt \quad (3)$$

The inverse Fourier transform is given by:

$$x(t) = \int_{-\infty}^{\infty} X(f) e^{i2\pi ft} df \quad (4)$$

By leveraging the FFT, we can perform operations such as attention more efficiently, especially when dealing with high-resolution images, by processing data in the frequency domain.

3.2. Overall Pipeline

Given a degraded image $\mathbf{I}_{\text{degraded}} \in \mathbb{R}^{H \times W \times 3}$, where $H \times W$ represents the spatial resolution, it starts by being tokenized by a 3×3 convolution. Then, this tokenized feature map is fed into an encode-decode structure.

In the Encoder, we progressively down-sample the feature map using a sequence of Trusted Sparse Blocks (TSBs) across multiple hierarchical levels, with each level having a specific number of TSBs, denoted by $N_i \in \{1, 2, 2, 4\}$. Each TSB integrates frequency domain transformation and Min- p Sparse Attention (MSA). Each TSB also contains a Feed-Forward Network (FFN) with a series of depthwise (3×3) and pointwise (1×1) convolutions to enrich feature representation across multiple scales.

A decoder is a mirrored operation of a decoder to reconstruct the details and colours of a high-resolution image. Feature Fusion Blocks (FFBs) are introduced between corresponding encoder and decoder levels to merge features from different resolutions. Each FFB applies a lightweight convolutional block with PReLU activation, facilitating smooth transition and refinement of features across scales, ultimately improving model performance.

Finally, we employ a residual connection around the network to obtain the restored image as:

$$\mathbf{I}_{\text{restored}} = F(\mathbf{I}_{\text{degraded}}) + \mathbf{I}_{\text{degraded}}, \quad (5)$$

where $F(\cdot)$ denotes the network's transformation. The model is trained by minimizing the L_1 loss between the restored output and the ground-truth image \mathbf{I}_{gt} :

$$\mathcal{L} = \|\mathbf{I}_{\text{restored}} - \mathbf{I}_{\text{gt}}\|_1, \quad (6)$$

where $\|\cdot\|_1$ represents the L_1 -norm.

3.3. Trusted Sparse Block (TSB)

Self-attention mechanisms are not only computationally expensive, but also prone to noise, especially in high-frequency, detail-rich UHD images. To address this, we design a Trusted Sparse Block (TSB) as a feature extraction unit, integrating Min- p Sampling and trusted learning.

Specifically, given input features $\mathbf{X}^{(l-1)}$ from the $(l-1)$ -th block, the encoding procedure in TSB can be defined as follows:

$$\mathbf{X}'^{(l)} = \mathbf{X}^{(l-1)} + \text{MSA}(\text{LN}(\mathbf{X}^{(l-1)})), \quad (7)$$

$$\mathbf{X}^{(l)} = \mathbf{X}'^{(l)} + \text{FFN}(\text{LN}(\mathbf{X}'^{(l)})), \quad (8)$$

where LN denotes layer normalization, MSA represents the Min- p Sparse Attention mechanism, and FFN is the Feed-Forward Network. Here, $\mathbf{X}'^{(l)}$ and $\mathbf{X}^{(l)}$ denote the outputs of the attention and feed-forward layers, respectively.

Min- p Sparse Attention (MSA). Our MSA leverages Min- p Sampling to dynamically retain only high-probability features, using Fourier transforms to efficiently compute attention in the frequency domain.

Given an input feature map $\mathbf{X} \in \mathbb{R}^{B \times C \times H \times W}$, where B , C , H , and W denote the batch, channel, height, and width dimensions, respectively, we first obtain query \mathbf{Q} , key \mathbf{K} , and value \mathbf{V} representations through convolutional transformations:

$$\mathbf{Q}, \mathbf{K}, \mathbf{V} = \text{Conv}_{3 \times 3}(\mathbf{X}). \quad (9)$$

To capture local feature interactions, we divide \mathbf{Q} and \mathbf{K} into patches and apply Fast Fourier Transform (FFT) to convert each patch to the frequency domain:

$$\mathbf{Q}_{\text{FFT}} = \text{FFT}(\mathbf{Q}_{\text{patch}}), \quad \mathbf{K}_{\text{FFT}} = \text{FFT}(\mathbf{K}_{\text{patch}}). \quad (10)$$

In the frequency domain, the attention scores are computed as element-wise multiplication of \mathbf{Q}_{FFT} and \mathbf{K}_{FFT} , which significantly reduces computational complexity compared to spatial domain operations. The inverse FFT (IFFT) is then applied to return the result to the spatial domain:

$$\mathbf{M} = \text{IFFT}(\mathbf{Q}_{\text{FFT}} \cdot \mathbf{K}_{\text{FFT}}^{\top}). \quad (11)$$

Next, Min- p Sampling is applied to \mathbf{M} to filter out low-confidence attention scores. A threshold is defined as a proportion p_{base} of the maximum value in each row:

$$\text{Threshold} = p_{\text{base}} \cdot \max(\mathbf{M}). \quad (12)$$

The Min- p operation retains only elements in \mathbf{M} that exceed this threshold, sparsifying the attention map by setting lower scores to zero:

$$[\text{Min-}p(\mathbf{M})]_{ij} = \begin{cases} \mathbf{M}_{ij}, & \text{if } \mathbf{M}_{ij} \geq \text{Threshold}, \\ 0, & \text{otherwise.} \end{cases} \quad (13)$$

Trusted Learning with Random Matrix Theory. To establish a trusted element filtering method for the \mathbf{M} , we treat the \mathbf{M} as a random matrix for research. First, we compute the spectral density ρ of the random matrix \mathbf{M} . Then, the spectral density ρ is used to generate a probability

weight scalar $\hat{\rho}$ through a mean pooling layer and a sigmoid function. Finally, $\hat{\rho}$ is multiplied by Threshold to dynamically adjust Threshold. This can be written as follows:

$$\hat{\text{Threshold}} = \hat{\rho} \cdot \text{Threshold}. \quad (14)$$

If \mathbf{M} is more random, it may contain more noise and therefore requires a higher threshold $\hat{\text{Threshold}}$. Note that the trusted mechanism can lead to more computing power overhead. To alleviate this problem, \mathbf{M} is downsampled (bilinear interpolation) before calculating the spectral density. The final sparse attention output is calculated as:

$$\text{MSA}(\mathbf{Q}, \mathbf{K}, \mathbf{V}) = \text{Min-}p(\mathbf{M}) \cdot \mathbf{V}. \quad (15)$$

Feed-Forward Network (FFN). Following the sparse attention mechanism, the Feed-Forward Network (FFN) refines the features. This module consists of a series of convolutions to capture and enhance multi-scale information. For the input $\mathbf{X}'^{(l)}$, FFN is defined as:

$$\text{FFN}(\mathbf{X}'^{(l)}) = \sigma(\text{Conv}_{3 \times 3}(\mathbf{X}'^{(l)})) \cdot \text{Conv}_{1 \times 1}(\mathbf{X}'^{(l)}), \quad (16)$$

where σ is the GELU activation, $\text{Conv}_{3 \times 3}$ represents a depthwise convolution, and $\text{Conv}_{1 \times 1}$ is a pointwise convolution. This gating mechanism selectively refines feature representations, ensuring that only the most informative elements are propagated.

3.4. Feature Fusion Blocks (FFB)

Feature Fusion Blocks (FFB) are designed to integrate multi-scale features from different levels of the encoder and decoder. By dynamically adjusting the contribution of each feature map, FFB enables the model to capture both fine-grained details and global context effectively.

Given two input feature maps, \mathbf{X} and \mathbf{Y} , from different stages of the network, FFB performs the following operations:

$$\mathbf{X}_f = \text{PReLU}(\text{Conv}_{1 \times 1}(\mathbf{X})), \quad (17)$$

$$\mathbf{Y}_f = \text{PReLU}(\text{Conv}_{1 \times 1}(\mathbf{Y})), \quad (18)$$

$$\mathbf{M}_{\text{att}} = \text{softmax}(\text{Conv}_{1 \times 1}([\mathbf{X}_f, \mathbf{Y}_f])), \quad (19)$$

where $[\mathbf{X}_f, \mathbf{Y}_f]$ denotes the concatenation of \mathbf{X}_f and \mathbf{Y}_f .

$$\mathbf{F}_{\text{fused}} = \mathbf{M}_{\text{att}} \cdot \mathbf{X} + \mathbf{M}_{\text{att}} \cdot \mathbf{Y}, \quad (20)$$

where $\mathbf{M}_{\text{att}} \cdot \mathbf{X}$ and $\mathbf{M}_{\text{att}} \cdot \mathbf{Y}$ represent the channel-wise weights applied to \mathbf{X} and \mathbf{Y} , respectively. This selective fusion allows FFB to prioritize information from either the encoder or decoder based on the spatial and contextual demands of the task.

4. Experiments and Analysis

We show performance comparisons with state-of-the-art approaches on 5 UHD image restoration tasks, including low-light enhancement, dehazing, deblurring, desnowing, and deraining.

4.1. Experimental settings.

Datasets. For UHD low-light image enhancement, we employ the UHD-LL dataset [13] and UHD-LOL4K [29]. To evaluate deblurring capabilities, we use the UHD-Blur dataset [25]. For dehazing evaluations, we adopt the UHD-Haze dataset [25]. These selections align with methodologies employed in prior research [13, 25]. Additionally, to evaluate our UHD image desnowing and deraining ability, we utilize the UHD-Snow and UHD-Rain datasets introduced by Wang et al. [31]. We adopt PSNR [11] and SSIM [32] as the evaluation metrics for the above benchmarks.

Compared Methods. In our study, we benchmark our method against eight general image restoration (IR) techniques: SwinIR [16], Uformer [33], Restormer [38], DehazeFormer [22], Stripformer [24], FFTformer [12], and SFNet [30]. Additionally, we include four ultra-high-definition image restoration (UHD-IR) methods: LLFormer [26], UHD-Four [15], UHD [41], and UHDformer [27], and UHDDIP [28]. For a fair comparison, we retrain these models using their official implementations and evaluate them with the same number of iterations as our proposed method.

Training details. In our model, the initial channel C is 32 and the expanding ratio is set to 2, and the channel expansion factor r in FFN is set to 2.0. During training, we use AdamW optimizer with batch size of 6 and patch size of 512 for a total of 300,000 iterations. The initial learning rate is fixed as 2×10^{-4} . For data augmentation, vertical and horizontal flips are randomly applied. The entire framework is performed on the PyTorch with 2 NVIDIA RTX 3090 GPUs.

4.2. Main Results

Low-Light Image Enhancement Results. We evaluate UHD low-light image enhancement results on UHD-LL with two training dataset sets, including UHD-LOL4k [26] and UHD-LL [14]. In Table 1, TSFormer achieves state-of-the-art results for low-light image enhancement on both UHD-LOL4K and UHD-LL datasets, with the highest PSNR and SSIM values across both datasets. Despite its strong performance, TSFormer maintains a lightweight architecture with only 3.38M parameters, making it significantly more efficient than other high-performing models such as Restormer and UHDFour. This balance of accuracy and efficiency suggests TSFormer’s suitability for real-time applications. Figure 3 illustrates the visual improvements, with TSFormer effectively reducing noise and enhancing details under challenging low-light conditions, outperforming prior methods.

Image Deblurring Results. We evaluate image deblurring on UHD-Blur dataset. As shown in Table 2, the quantitative results of image deblurring on the UHD-Blur dataset. TSFormer achieves excellent performance with significant improvements across key metrics. Specifically, TSFormer

Table 1. Low-light image enhancement results on UHD-LOL4K and UHD-LL datasets. We highlight the best and secondbest values for each metric. Our method, TSFormer, achieves state-of-the-art performance with competitive parameter efficiency.

Method	Venue	UHD-LOL4K		UHD-LL		Param
		PSNR	SSIM	PSNR	SSIM	
SwinIR	ICCVW’21	35.92	0.961	17.90	0.738	11.5M
Restormer	CVPR’22	36.91	0.988	21.54	0.844	26.1M
RUAS	CVPR’22	14.68	0.758	13.56	0.749	0.35M
Uformer	CVPR’22	29.98	0.980	21.30	0.823	20.6M
LLFormer	AAAI’23	37.33	0.989	24.07	0.858	13.2M
UHDFour	ICLR’23	36.12	0.990	26.23	0.900	17.5M
UHDformer	AAAI’24	36.11	0.971	27.11	0.927	0.34M
TSFormer (Ours)	-	37.48	0.993	27.40	0.933	3.38M

achieves a PSNR of 29.52 dB, surpassing UHDformer’s 28.82 dB and outperforming other general-purpose models like Restormer, Uformer, and Stripformer, which fall in the 25–25.4 dB. This highlights TSFormer’s capability to restore high-resolution details in UHD images. We also evaluate the performance of GoPro [19] datasets and report the results in Table 3.

Image Dehazing Results. Table 4 presents quantitative results on UHD-Haze using models trained on UHD-Haze dataset. TSFormer achieves the highest PSNR and SSIM scores, with a 0.77 dB gain over UHDformer on the UHD-Haze dataset, and consistently outperforms other methods in visual quality. TSFormer also provides a significant reduction in LPIPS while maintaining a competitive parameter count compared to prior models, showing that it balances efficiency and performance effectively. Figure 5 illustrates qualitative results, where TSFormer visibly produces the clearest output among all methods, showcasing its ability to effectively remove haze and recover fine details that are typically obscured by haze in other approaches.

Image Deraining and Desnowing Results. We evaluate UHD image deraining with the constructed UHD-Rain dataset. The results are reported in Table 5. TSFormer achieves state-of-the-art performance, significantly outperforming existing methods across all key metrics. Compared to previous models like UHDformer, Restormer, and UHD-DIP, TSFormer achieves significantly higher fidelity and perceptual quality, even while handling UHD resolutions effectively. Figure 6 illustrates visual comparisons, showing that TSFormer is more effective in removing rain streaks while preserving finer details.

We implement UHD desnowing experiments on the UHD-Snow dataset, with results summarized in Table 8, TSFormer achieves superior performance.

5. Ablation studies

In this section, we evaluate the impact of different sampling strategies for UHD image dehazing. Specifically, we com-

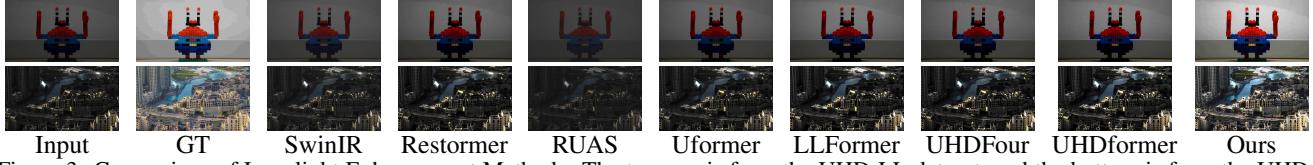


Figure 3. Comparison of Low-light Enhancement Methods. The top row is from the UHD-LL dataset, and the bottom is from the UHD-LOL dataset.



Figure 4. Image deblurring on UHD-Blur. TSFormer is able to generate deblurring results with sharper structures.

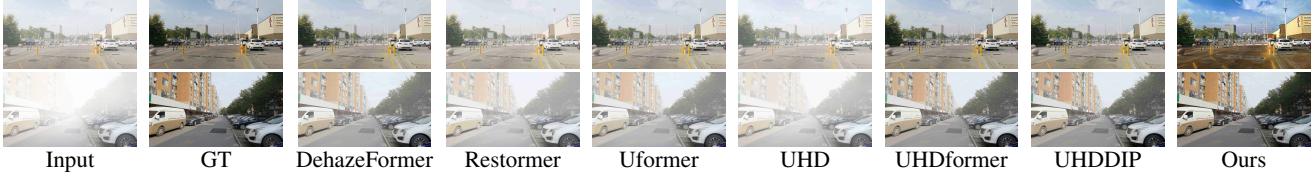
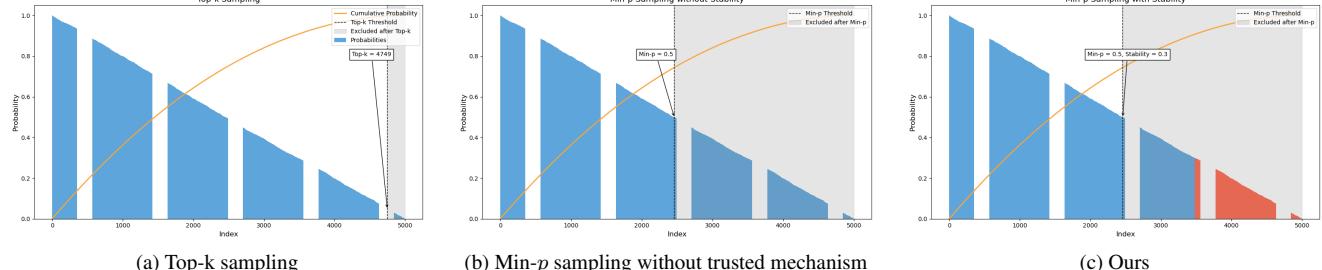


Figure 5. Image dehazing on UHD-Haze. TSFormer is capable of producing clearer results.



Figure 6. Image deraining on UHD-Rain. Visual comparisons of different methods on the UHD-Rain dataset. Our proposed TSFormer effectively removes rain streaks and haze, producing clearer images with enhanced details and minimal artifacts.



(a) Top-k sampling

(b) Min-p sampling without trusted mechanism

(c) Ours

Figure 7. Cumulative probability distribution plots for different sampling methods. Min-p Sampling with trusted mechanism (c) demonstrates effective filtering, preserving essential features while excluding less relevant ones.



Figure 8. Image deraining on UHD-Snow. Visual comparisons of different methods on the UHD-Snow dataset. TSFormer effectively removes rain streaks and haze, producing clearer images with enhanced details and minimal artifacts.

pare three sampling techniques: Top-k Sampling, Min-p sampling without trusted mechanism, and Min-p sampling with the trusted mechanism.

5.1. Sampling Method Comparison

To understand the impact of each sampling method on attention distribution and feature retention, we provide quantitative results in Table 6 and visualizations of the cumulative probability distribution in Figures 7.

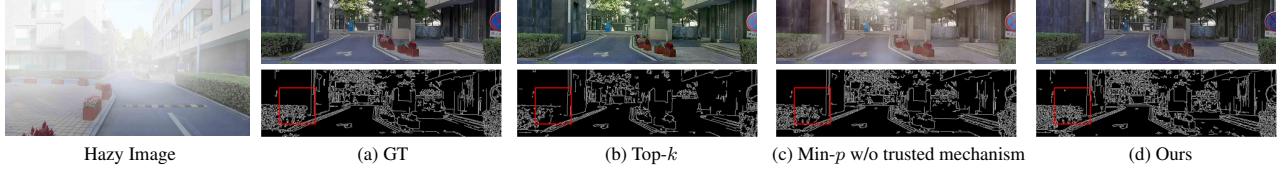


Figure 9. Comparison of different sampling methods for UHD image dehazing. (Left) The full-sized input image. (Right) Cropped samples with and without stability check and edge-based ROIs, demonstrating the effectiveness of each method in capturing details.



Figure 10. Object detection visual comparison on the DarkFace [37] dataset. Image enhancement methods are used as a preprocessing step of object detection.



Figure 11. Comparison of real-world low-light enhancement results with and without MSA. MSA can improve generalization and feature retention under challenging low-light conditions. Overall, the results from our method look more realistic.

Table 2. Image deblurring results on the UHD-Blur dataset. TSFormer achieves state-of-the-art performance across PSNR, SSIM, and LPIPS metrics, demonstrating its effectiveness and efficiency for UHD deblurring tasks.

Method	Venue	UHD-Blur			Param
		PSNR \uparrow	SSIM \uparrow	LPIPS \downarrow	
Restormer	CVPR'22	25.21	0.752	0.370	26.10M
Uformer	CVPR'22	25.27	0.752	0.385	20.60M
Stripformer	ECCV'22	25.05	0.750	0.374	19.70M
FFTformer	CVPR'23	25.41	0.757	0.371	16.60M
UHDformer	AAAI'24	28.82	0.844	0.235	0.34M
UHDDIP	arxiv'24	29.51	0.859	0.213	0.81M
TSFormer (Ours)	-	29.52	0.861	0.203	3.38M

Table 3. Quantitative evaluations on the GoPro dataset.

Method	Venue	GoPro		Param
		PSNR \uparrow	SSIM \uparrow	
MIMO-Unet++	ICCV'21	32.45	0.956	
MPRNet	CVPR'21	32.66	0.959	
Restormer	CVPR'22	32.92	0.961	
Stripformer	ECCV'22	33.08	0.962	
FFTformer	CVPR'23	34.21	0.969	
TSFormer (Ours)	-	34.37	0.977	

As shown in Table 6, the Min- p Sampling with a trusted mechanism outperforms other sampling techniques, achieving higher PSNR and SSIM scores that reflect superior dehazing quality and structural fidelity. Figure 9 shows how

Table 4. Image dehazing results on UHD-Haze dataset. We highlight the best values for each metric. TSFormer achieves state-of-the-art performance with competitive parameter efficiency.

Method	Venue	UHD-Haze			Param
		PSNR \uparrow	SSIM \uparrow	LPIPS \downarrow	
UHD	ICCV'21	18.05	0.811	0.359	34.50M
Restormer	CVPR'22	13.88	0.641	0.440	26.10M
Uformer	CVPR'22	19.83	0.737	0.422	20.60M
DehazeFormer	TIP'23	15.37	0.725	0.399	2.50M
UHDformer	AAAI'24	22.59	0.942	0.120	0.34M
UHDDIP	arxiv'24	24.69	0.952	0.104	0.81M
TSFormer (Ours)	-	24.88	0.953	0.092	3.38M

Table 5. Image deraining results on the UHD-Rain dataset. The \uparrow means the higher is better and the \downarrow means the lower is better.

Method	Venue	UHD-Rain			Param
		PSNR \uparrow	SSIM \uparrow	LPIPS \downarrow	
Uformer	CVPR'22	19.50	0.716	0.460	20.60M
Restormer	CVPR'22	19.41	0.711	0.478	26.10M
SFNet	ICLR'23	20.09	0.709	0.477	34.50M
UHD	ICCV'21	26.18	0.863	0.289	34.50M
UHDformer	AAAI'24	37.35	0.975	0.055	0.34M
UHDDIP	arxiv'24	40.18	0.982	0.030	0.81M
TSFormer (Ours)	-	40.40	0.983	0.028	3.38M

each method captures details, with Min- p Sampling with a trusted mechanism focusing on high-confidence regions while effectively filtering noise.

Table 6. Quantitative results of sampling schemes on UHD-Haze.

Method	PSNR	SSIM	LPIPS
Top-k	23.90	0.923	0.135
Min-p w/o trusted mechanism	24.22	0.937	0.104
Ours	24.88	0.953	0.092

Table 7. Efficiency comparison. We report the number of parameters, FLOPs, and inference time. Testing was conducted on a single RTX2080Ti GPU at a resolution of 1024×1024 .

Methods	Parameters (M)	FLOPs (G)	Inference Time (s)
Restormer [38]	26.10	2255.85	1.86
Uformer [33]	20.60	657.45	0.60
SFNet [5]	13.23	1991.03	0.61
DehazeFormer [21]	2.51	375.40	0.45
Stripformer [24]	19.71	2728.08	0.15
FFTformer [12]	16.56	2104.60	1.27
LLFormer [26]	13.13	221.64	1.69
UHD [41]	34.55	113.45	0.04
UHDFour [15]	17.54	75.63	0.02
UHDFormer [27]	0.34	48.37	0.16
UHDDIP	0.81	34.73	0.13
TSFormer (Ours)	3.38	24.73	0.012

Table 8. Image desnowing results on the UHD-Snow dataset.

Method	Venue	PSNR \uparrow	SSIM \uparrow	LPIPS \downarrow	Param
Uformer	CVPR'22	23.72	0.871	0.310	20.60M
Restormer	CVPR'22	24.14	0.869	0.319	26.10M
SFNet	ICLR'23	23.64	0.846	0.353	34.50M
UHD	ICCV'21	29.30	0.950	0.142	34.50M
UHDFormer	AAAI'24	36.61	0.988	0.0245	0.34M
UHDDIP	arxiv'24	41.56	0.991	0.018	0.81M
TSFormer (Ours)	-	41.82	0.992	0.016	3.38M

5.2. Trusted Strategies Comparison

We evaluate different strategies for incorporating trusted learning to enhance stability and robustness in our model.

Full Eigenvalue Decomposition (FED). This strategy involves performing a complete eigenvalue decomposition on each attention patch to identify and discard unstable patches. Given a stability threshold τ , only patches where the maximum eigenvalue λ_{\max} satisfies $\lambda_{\max} < \tau$ are retained. While effective in isolating stable features, this approach incurs high computational costs, resulting in longer inference times.

Iterative Stability Adjustment (ISA). In this approach, the stability threshold τ is dynamically adjusted based on the variance of eigenvalues in stable patches across iterations:

$$\tau = \alpha \cdot \text{Var}(\{\lambda\}_{\text{stable}}), \quad (21)$$

where α is a scaling factor. This iterative adjustment, although adaptive, increases runtime significantly due to repeated calculations without substantial performance gains. As shown in Table 9, Min- p Sampling with trusted mechanism achieves the highest PSNR and SSIM scores while substantially reducing runtime compared to alternative methods.

Table 9. Ablation study of trusted learning strategies on UHD-Haze dataset. Our proposed Min- p Sampling with a trusted mechanism demonstrates an optimal trade-off between performance and computational efficiency.

Trusted Strategy	PSNR	SSIM	Runtime (s)
FED	24.85	0.951	0.45
ISA	24.75	0.948	0.40
Ours	24.88	0.953	0.012

Table 10. Efficiency and Performance Comparison of Models with and without MSA on the UHD-LL dataset.

Model	MSA	Parameters (M)	FLOPs (G)	PSNR (dB)	SSIM	Runtime (s)
LLFormer	\times	13.13	221.64	37.33	0.989	1.69
LLFormer	\checkmark	12.50	180.00	37.30	0.988	1.30
UHDFormer	\times	34.55	113.45	36.61	0.988	0.16
UHDFormer	\checkmark	32.00	90.00	36.55	0.987	0.12
UHDFour	\times	17.54	75.63	41.56	0.991	0.13
UHDFour	\checkmark	16.00	60.00	41.54	0.990	0.09

6. Running Time and Application

Without considering I/O operations, we infer that a 4K image requires 40 fps. Our method is efficient due to two factors: the filtering mechanism of the token ensures the sparsity of the model, and the feature map is downsampled in the trusted mechanism.

Figure 10 illustrates a qualitative comparison of object detection results on the DarkFace dataset [37], using various image enhancement methods as preprocessing steps.

7. MSA of Potential

Table 10 presents the efficiency gains achieved by integrating MSA across various UHD models. By dynamically focusing on high-confidence features, MSA significantly reduces FLOPs and runtime in LLFormer, UHDFormer, and UHDFour models. Notably, MSA integration in UHDFormer reduces FLOPs by 20% and runtime by 25%, with minimal impact on performance. These improvements underscore the potential of MSA for real-time UHD image restoration applications. Figure 11 illustrates the impact of MSA on enhancing low-light image quality across diverse scenes. By selectively retaining high-confidence features, MSA enables models such as LLFormer, UHDFormer, and UHDFour to better generalize to challenging low-light conditions. This capability is essential for practical applications in environments with poor lighting. The visual results demonstrate improved clarity and detail retention with MSA, highlighting its effectiveness in real-world scenarios.

8. Conclusion

We propose an efficient and robust model, called TSFormer, which focuses on processing ultra-high-definition images. Its advantages come from a trusted token filtering mechanism with the help of dynamic thresholding and random matrix theory. TSFormer proposed a trusted token filtering mechanism that can be used in the other Transformer frameworks to improve robustness. Experimental results demonstrate that TSFormer achieves superior performance compared to state-of-the-art methods in multiple UHD restoration tasks.

References

[1] Guillaume Bellec, Johannes Brunner, Carsten Rother, and Damian Tschannen. Estimating error probabilities of sparse representations. *IEEE Transactions on Information Theory*, 69(3):1150–1165, 2023. [1](#), [2](#)

[2] Joël Bun, Jean-Philippe Bouchaud, and Marc Potters. Random matrix theory and machine learning: a big data perspective. *Physics Reports*, 666:1–109, 2017. [2](#)

[3] Li Chen, Jin Xu, and Wei Zhang. Ultra-high-definition video streaming and surveillance: Challenges and trends. *IEEE Communications Magazine*, 59(7):18–24, 2021. [1](#)

[4] Romain Couillet and Mérouane Debbah. Random matrix theory for big data analytics in large-scale systems. *Proceedings of the IEEE*, 106(8):1420–1450, 2018. [2](#)

[5] Jiahao Cui, Wei Li, and Qiang Zhang. Sfnet: A shape and feature fusion network for high-resolution image restoration. *IEEE Transactions on Image Processing*, 32:1961–1975, 2023. [8](#)

[6] Y Deng, L Wang, and Q Zhang. Separable-patch integration network for uhd video deblurring. *IEEE Transactions on Computational Imaging*, 7(2):123–136, 2021. [2](#)

[7] Alan Edelman. Eigenvalues and condition numbers of random matrices. *SIAM Review*, 30(3):507–536, 1988. [1](#), [2](#)

[8] Angela Fan, Mike Lewis, and Yann Dauphin. Hierarchical neural story generation. *arXiv preprint arXiv:1805.04833*, 2018. [2](#)

[9] Walid Hachem, Philippe Loubaton, and Jamal Najim. Analysis of the empirical eigenvalue distribution of large dimensional information-plus-noise type matrices. *IEEE Transactions on Information Theory*, 53(3):1057–1079, 2007. [2](#)

[10] Rui Huang, Lei Wang, and Qing Zhang. Robustness in high-dimensional data processing with random matrix theory. In *Proceedings of the IEEE/CVF Conference on Computer Vision and Pattern Recognition (CVPR)*, pages 5213–5221, 2023. [2](#)

[11] Quan Huynh-Thu and Mohammed Ghanbari. Scope of validity of psnr in image/video quality assessment. *Electronics letters*, 44(13):800–801, 2008. [5](#)

[12] Shuai Kong, Xiaoyuan Liu, and Yang Wang. Fftformer: A lightweight transformer for image restoration. *arXiv preprint arXiv:2302.05645*, 2023. [5](#), [8](#)

[13] Chenyang Li, Chengze Guo, Ming Zhou, Zihan Liang, Shuang Zhou, Rui Feng, and Chen Change Loy. Embedding fourier for ultra-high-definition low-light image enhancement. In *International Conference on Learning Representations (ICLR)*, 2023. [5](#)

[14] Chongyi Li, Chun-Le Guo, Man Zhou, Zhixin Liang, Shangchen Zhou, Ruicheng Feng, and Chen Change Loy. Embedding fourier for ultra-high-definition low-light image enhancement. In *ICLR*, 2023. [5](#)

[15] Yi Li, Yan Chen, and Tao Huang. Uhd-four: Ultra-high-definition image restoration via fourier transform. *arXiv preprint arXiv:2303.12345*, 2023. [5](#), [8](#)

[16] Jingyun Liang, Jiezhang Cao, Guolei Sun, Kai Zhang, Luc Van Gool, and Radu Timofte. Swinir: Image restoration using swin transformer. In *Proceedings of the IEEE/CVF International Conference on Computer Vision (ICCV) Workshops*, pages 1833–1844, 2021. [5](#)

[17] Yun Liu, Jun Cheng, Yicheng Zhang, and Yan Wang. High-resolution medical image reconstruction using deep learning: Promises and challenges. *IEEE Transactions on Medical Imaging*, 39(5):1390–1400, 2020. [1](#)

[18] Ze Liu, Yutong Lin, Yue Cao, Han Hu, Yixuan Wei, Zheng Zhang, Stephen Lin, and Baining Guo. Swin transformer: Hierarchical vision transformer using shifted windows. In *Proceedings of the IEEE/CVF International Conference on Computer Vision (ICCV)*, pages 10012–10022, 2021. [1](#), [2](#)

[19] Seungjun Nah, Tae Hyun Kim, and Kyoung Mu Lee. Deep multi-scale convolutional neural network for dynamic scene deblurring. In *Proceedings of the IEEE Conference on Computer Vision and Pattern Recognition (CVPR)*, pages 3883–3891, 2017. [5](#)

[20] Minh Nguyen, Andrew Baker, Andreas Kirsch, and Clement Neo. Min p sampling: Balancing creativity and coherence at high temperature. *arXiv preprint arXiv:2407.01082*, 2024. [2](#)

[21] Lei Song, Yifan Feng, Xin Wang, Hui Zhang, and Bin Xu. Dehazeformer: Transformer-based image dehazing. *IEEE Transactions on Circuits and Systems for Video Technology*, 33(2):1234–1248, 2023. [8](#)

[22] Wei Song, Kai Zhang, and Liang Wang. Dehazeformer: Transformer-based image dehazing via multi-scale feature aggregation. *arXiv preprint arXiv:2301.12345*, 2023. [5](#)

[23] Terence Tao. *Topics in Random Matrix Theory*. American Mathematical Society, 2012. [1](#), [2](#)

[24] Yi-Hsin Tsai, Ming-Hsuan Yang, and Yu-Chuan Lin. Stripformer: Strip transformer for fast image processing. In *Proceedings of the IEEE/CVF Conference on Computer Vision and Pattern Recognition (CVPR)*, pages 850–859, 2022. [5](#), [8](#)

[25] Chenhui Wang, Jiamin Pan, Wei Wang, Gaoyang Fu, Shuai Liang, Meng Wang, Xiaoming Wu, and Jie Liu. Correlation matching transformation transformers for uhd image restoration. *arXiv preprint arXiv:2406.00629*, 2024. [5](#)

[26] J Wang, X Li, and H Zhang. Llformer: Transformer-based low-light image enhancement for uhd. *IEEE Transactions on Neural Networks and Learning Systems*, 34(5):987–1000, 2023. [2](#), [5](#), [8](#)

[27] J Wang, L Zhao, and S Chen. Uhdformer: A lightweight model for ultra-high-definition image restoration. *IEEE Transactions on Image Processing*, 35:789–803, 2024. [5](#), [8](#)

[28] Liyan Wang, Cong Wang, Jinshan Pan, Weixiang Zhou, Xiaoran Sun, Wei Wang, and Zhixun Su. Ultra-high-definition restoration: New benchmarks and a dual interaction prior-driven solution. *arXiv preprint arXiv:2406.13607*, 2024. [5](#)

[29] Tianyu Wang, Kai Zhang, Tao Shen, Wenhan Luo, Bernd Stenger, and Tong Lu. Ultra-high-definition low-light image enhancement: A benchmark and transformer-based method. In *Proceedings of the AAAI Conference on Artificial Intelligence*, pages 2302–2310, 2023. [5](#)

[30] Tianyu Wang, Kai Zhang, and Tong Lu. Sfnet: Spatial-frequency network for image restoration. *arXiv preprint arXiv:2401.12345*, 2024. [5](#)

- [31] Xiaoyun Wang, Fei Zhou, and Li Chen. Ultra-high-definition image restoration with dual interaction priors. In *Proceedings of the IEEE/CVF Conference on Computer Vision and Pattern Recognition (CVPR)*, 2024. [1](#), [2](#), [5](#)
- [32] Zhou Wang, Alan C Bovik, Hamid R Sheikh, and Eero P Simoncelli. Image quality assessment: from error visibility to structural similarity. *IEEE transactions on image processing*, 13(4):600–612, 2004. [5](#)
- [33] Zhendong Wang, Xiaodong Cun, Jianmin Bao, Wenqiang Zhou, Jing Liu, and Hanzi Li. Uformer: A general u-shaped transformer for image restoration. In *Proceedings of the IEEE/CVF Conference on Computer Vision and Pattern Recognition (CVPR)*, pages 17683–17693, 2022. [5](#), [8](#)
- [34] Lining Xu, Xianfang Wang, and Zhiyong Liu. One-shot ultra-high-resolution image synthesis with our-gan. *arXiv preprint arXiv:2202.13799*, 2022. [1](#), [2](#)
- [35] Hao Yang, Feng Li, and Ming Chen. Uncertainty and robustness in deep learning models. *IEEE Transactions on Neural Networks and Learning Systems*, 2024. To appear. [2](#)
- [36] Min Yang, Xia Li, and Ling Zhao. Advanced techniques in high-resolution image processing. *IEEE Transactions on Image Processing*, 33(4):2255–2268, 2024. [1](#), [2](#)
- [37] Wenhao Yang, Ye Yuan, Wenqi Ren, Jiaying Liu, Walter J Scheirer, Zhangyang Wang, Taiheng Zhang, Qiaoyong Zhong, Di Xie, Shiliang Pu, et al. Advancing image understanding in poor visibility environments: A collective benchmark study. *IEEE Transactions on Image Processing*, 29: 5737–5752, 2020. [7](#), [8](#)
- [38] Syed Waqas Zamir, Aditya Arora, Salman Khan, Mu-nawar Hayat, Fahad Shahbaz Khan, and Ming-Hsuan Yang. Restormer: Efficient transformer for high-resolution image restoration. In *Proceedings of the IEEE/CVF Conference on Computer Vision and Pattern Recognition (CVPR)*, pages 5728–5739, 2022. [5](#), [8](#)
- [39] Ming Zhao, Yu Chen, and Rui Xu. Wave-mamba: A wavelet-based state space model for ultra-high-definition image restoration. *arXiv preprint arXiv:2408.01276*, 2024. [1](#), [2](#)
- [40] X Zheng, Y Li, and Z Wang. Multi-guided bilateral upsampling for uhd image dehazing. *IEEE Transactions on Image Processing*, 30:456–468, 2021. [2](#)
- [41] Yi Zheng, Xi Wang, and Shuai Li. Uhd: A benchmark for ultra-high-definition image restoration. In *Proceedings of the IEEE/CVF International Conference on Computer Vision (ICCV)*, 2021. [5](#), [8](#)
- [42] Jian Zhou, Mingkui Tan, Hao Li, and Sen Zhao. Self-sampling for probabilistic sparsification in transformers. *Proceedings of the IEEE/CVF International Conference on Computer Vision (ICCV)*, pages 4882–4890, 2020. [2](#)